PNAS
www.pnas.org

Supplementary Information for

Bladder drug mirabegron exacerbates atherosclerosis through activation of brown fat-mediated lipolysis

Wenhai Sui[1,2], Hongshi Li[1], Yunlong Yang[3], Xu Jing[4], Fei Xue[1], Jing Cheng[1], Mei Dong[1], Meng Zhang[1], Huazheng Pan[5], Yuguo Chen[6], Yunjian Zhang[7], Qingjun Zhou[8], Weiyun Shi[8], Xinsheng Wang[9], Han Zhang[10], Cheng Zhang[1], Yun Zhang[1,*] and Yihai Cao[2*]

[1]The Key Laboratory of Cardiovascular Remodeling and Function Research, Chinese Ministry of Education, Chinese National Health Commission and Chinese Academy of Medical Sciences, The State and Shandong Province Joint Key Laboratory of Translational Cardiovascular Medicine, Department of Cardiology, Qilu Hospital of Shandong University, Jinan, 250012, China

[2]Department of Microbiology, Tumor and Cell Biology, Karolinska Institute, 171 77 Stockholm, Sweden

[3]Department of Cellular and Genetic Medicine, School of Basic Medical Sciences, Fudan University, Shanghai 200032, China.

[4]Department of Clinical Laboratory, The Second Hospital of Shandong University, Jinan, Shandong 250012, China.

[5]Clinical Laboratory, The Affiliated Hospital of Qingdao University, Qingdao, China.

[6]Department of Emergency, Qilu Hospital of Shandong University, Jinan, Shandong 250012, China

[7]Department of Thyroid and Breast Surgery, the First Affiliated Hospital of Sun Yat-sen University, Guangzhou, China.

www.pnas.org/cgi/doi/10.1073/pnas.1901655116

[8]State Key Laboratory Cultivation Base, Shandong Provincial Key Laboratory of Ophthalmology, Shandong Eye Institute, Shandong Academy of Medical Sciences, Yanerdao Road, Qingdao, 266071, China.

[9]Central Research Laboratory, The Affiliated Hospital of Qingdao University, Qingdao, 266071, China.

[10] Key Laboratory of Optoelectronic Devices and Systems of Ministry of Education and Guangdong Province, Shenzhen University, Shenzhen 518060, People's Republic of China.

*Correspondence, galley proofs and reprint requests should be primarily addressed to: Yihai Cao, M.D., Ph.D., Department of Microbiology, Tumor and Cell Biology, Karolinska Institutet, 171 77 Stockholm, Sweden. Tel: (+46)-8-52487596, Fax: (+46)-8-33 13 99, E-mail: yihai.cao@ki.se

This PDF file includes:

Supplementary text
Figs. S1 to S10
Tables S1
References for SI reference citations

Supplementary Information Text

Materials and Methods

Mirabegron treatment Mirabegron was purchased form BOC sciences (223673-61-8, NY, USA) and was dissolved in polyethylene glycol (PEG, 91893, Sigma-Aldrich, Shanghai, China) as a stock, which was further diluted in PBS upon use. Mirabegron was orally administrated in each mouse at 0.8 mg/kg weight/day as a low dose, and 8 mg/kg weight/day as a high dose. The low dose of mirabegron is equivalent to 50 mg/person of clinical dose used for treating overactive bladder syndrome. A solution containing an equal amount of PEG diluted in normal saline served as a vehicle. Vehicle, low- and high-dose of mirabegron were administrated to *wt* mice (n=15 per group) for 4 weeks. *ApoE*$^{-/-}$ and *Ldlr*$^{-/-}$ mice were fed with a high fat diet containing 40% fat and 1.25% cholesterol (TP28521, Trophic Animal Feed High-Tech Co., Ltd, Nantong, China) for 8 weeks. Mirabegron and vehicle treatment was initiated at the end of week 2 until the termination of experiments. After sacrifice, various tissue samples were collected, followed by fixation with 4% paraformaldehyde solution. A fraction of tissues was frozen in liquid nitrogen for further histological analysis.

RNA sequencing array WT mice (n=3 per group) were treated with mirabegron and vehicle for 4 days and subWAT was used to isolate RNA for RNA-seq assay. Total RNA was isolated using a RNeasy mini kit (74804, Qiagen, Germany). Paired-end libraries were synthesized using the SureSelect Strand-Specific RNA Component kit (Agilent, USA) according to the sample preparation guide. Purified libraries were quantified using the Qubit 2.0 Fluorometer (Life Technologies, USA) and validated by Agilent 2100 bioanalyzer (Agilent Technologies, USA) to calculate the insert size and concentrations. Clusters were generated using cBot with the library diluted to 10 pM, followed by sequencing on the NovaSeq 6000 (Illumina, USA). The library construction and sequencing were performed at the Shanghai Sinomics Corporation.

Antibodies A rabbit anti-mouse UCP1 (ab10983, Abcam, Cambridge, UK), a rabbit anti-mouse prohibitin (ab28172, Abcam, Cambridge, UK), a rabbit anti-mouse perilipin A (ab3526, Abcam, Cambridge, UK), a rabbit anti-mouse CD31 (ab28364, Abcam, Cambridge, UK), a rabbit anti-mouse PDGFRα (ab65258, Abcam, Cambridge, UK), a rabbit anti-mouse COX4 (ab202554, Abcam, Cambridge, UK), a rabbit anti-mouse α-SMA (ab5694, Abcam, Cambridge, UK), a rat anti-mouse F4/80 (MAB5580, R&D, Minneapolis, USA), a rat anti-mouse MOMA2 (MCA519G, BIO-RAD, California, USA), a rat anti-mouse endomucin (14-5851, eBioscience, San Diego, USA), and a mouse anti-β-actin (ZSGB-Bio, Beijing, China) were used as primary antibodies. The Horseradish Peroxidase (HRP)-conjugated secondary antibodies were used as followed: a rabbit anti-rat (ab6734, Abcam, Cambridge, UK) antibody, a goat anti-rabbit (ab97051, Abcam, Cambridge, UK) antibody, and a rabbit anti-mouse (ab97046, Abcam, Cambridge, UK) antibody. A donkey anti-rabbit (Alexa Fluor® 594, ab150076, Abcam, Cambridge, UK) was used for immunofluorescence. The HRP-DAB detection system (ZSGB-Bio, Beijing, China) was used for immunohistochemical staining.

Micro-PET-CT imaging Mice receiving various doses of Mirabegron were fasted 8 h before the scanning. 2-^{18}F-fluoro-2-deoxy-D-glucose (^{18}F-FDG) with the radiochemical purity more than 95 % was produced by a cyclotron (Siemens CTI RDS Eclips ST, Knoxville, TN) using the Explora FDG4 module.
In vivo PET/CT imaging scans and image analysis were performed using an Inveon Animal-PET/CT system (Siemens Preclinical Solution, Knoxville, TN). Mice receiving various doses of Mirabegron were scanned 1 h after *i.v.* injection of 200 μCi of ^{18}F-FDG. Animals were maintained with anesthetization using 2.5 % isoflurane/oxygen before and during the scanning. Three-dimensional ordered-subset expectation maximization (3D-OSEM)/maximum algorithm was used for image reconstruction. The max of percentage-injected dose per gram (%ID/gmax) was calculated, while standardized uptake value (SUV) by body weight (SUV-BW) of the iBAT was measured by manually drawn region of interest (ROI). Inveon Acquisition Workplace software (Siemens Medical Solutions) was used for analysis.

Histology and immunohistochemistry Hematoxylin and eosin staining was performed according to our previously published methods. Adipose depots embedded in paraffin were cut in 5-μm-thick slides. After dewaxing and antigen retrieval with a citrate buffer (pH 6.0), followed by treatment with 3% H_2O_2, tissue slides were blocked at room temperature with 5% non-immune goat serum for 60 min. Primary antibodies, including UCP1, prohibitin, perilipin A, CD31, PDGFRα, α-SMA, F4/80, MOMA2 and endomucin were incubated at 4°C overnight. A HRP-conjugated or an Alexa Fluor 594-labeled secondary antibody was added next day at room temperature for 1 h. A DAB kit (ZSGB-Bio, Beijing) was used for color development. The nuclei were counterstained with hematoxylin in immunohistochemical staining or DAPI in immunofluorescent staining. Aortas were stained in 0.5% Oil Red O (O0625, Sigma-Aldrich, Shanghai, China) at room temperature for 20 min, followed by washing at 37°C with PBS.

Blood sample collection Mice were starved for 8 h prior to measuring blood lipids and fasting insulin. Blood samples were collected by retro-orbital puncturing or through the cardiac apex of pentobarbital-anesthetized animals.

Real-time PCR Total RNA was extracted from adipose tissues using a RNeasy mini kit (74804, Qiagen, Germany) according to the manufacturer's instruction. cDNA was synthesized using a PrimeScript RT reagent Kit (0037, Takara, Japan). qPCR was performed using the UltraSYBR Mixture reagents (CWBiotech, Beijing, China) with a Roche LC480 system. The $2^{-\Delta\Delta CT}$method was used to assess relative mRNA expression levels. Primers were listed in **Supplementary Table 1**. Pooled liver tissues were used to prepare to RNA and cDNA for detection of *Hmgcr*, *Scap*, *Srebp1*, and *Srebp2* mRNA expression.

Western blot analysis Total proteins from adipose tissues were extracted by a Total Protein Extraction Kit (AT-022, Invent Biotechnologies, Inc. Plymouth USA), which was separated by SDS-PAGE electrophoresis, transferred to a PVDF membrane, blocked with 5% non-fat milk, and incubated with primary antibodies at 4°C overnight. Transferred blots were displayed using a chemiluminescent reagent (WBKLS0500, Millipore, Germany).

Indirect calorimetry After 3-week treatment with mirabegron, non-shivering thermogenesis (NST) was measured by an open-circuit system (Sable, USA) as previously described (1-3). Animals were anaesthetized with pentobarbital (90 mg/kg, i.p.) and oxygen consumption and carbon dioxide release were measured at 33°C for 30 min. After measuring the basal metabolic rate, mice were injected with norepinephrine (1 mg/kg, s.c.). O_2 consumption and CO_2 release were recorded for the consecutive 90 min.

Serum lipid analysis and FPLC chromatography Total cholesterol (TC), low-density lipoprotein cholesterol (LDL-C), triglyceride (TG), and free fatty acid (FFA) in serum were measured using commercial kits (Roche Diagnostics, Mannheim, Germany). Serum levels of very low-density lipoprotein (VLDL) were measured by an ELISA kit (E17089m, CUSABIO, Houston, USA). FPLC chromatography was used for detailed analysis of various cholesterol components and TG as described before (3). Briefly, an aliquot of 100 μl of plasma was chromatographed on a Sepharose 6 HR10/300 GL column (GE Healthcare, Sweden) and eluted with 1x PBS at a speed of 0.5 ml/min. A total number of 60 fractions (0.5 ml/fraction) were collected, and each fraction was analyzed for cholesterol and TG concentrations using standard ELISA Kits (Cayman, Florida). Values from fractions 5-10 were used for calculation of VLDL/IDL, whereas fractions 11-19 and fractions 20-30 represent LDL and HDL respectively.

Blood glucose, insulin, insulin tolerance test, and glucose tolerance test An accu Chek glucose meter and the matched blood glucose strips (Roche Diagnostics, Mannheim, Germany) were used to measure fasting glucose and to monitor blood glucose levels during insulin and glucose tolerance tests (4). For the insulin tolerance test, all mice were fasted for 8 h, followed by intraperitoneally injection with 0.5 U/kg human insulin. Blood glucose was monitored at post-injection time points of 0, 15, 30, 60, 90, and 120 min as described above. For the glucose tolerance test, all mice were fasted for 12 h and were intraperitoneally injected with 2 g/kg glucose. Blood glucose levels were monitored at post-injection time points of 0, 15, 30, 60, 90, and 120 min.

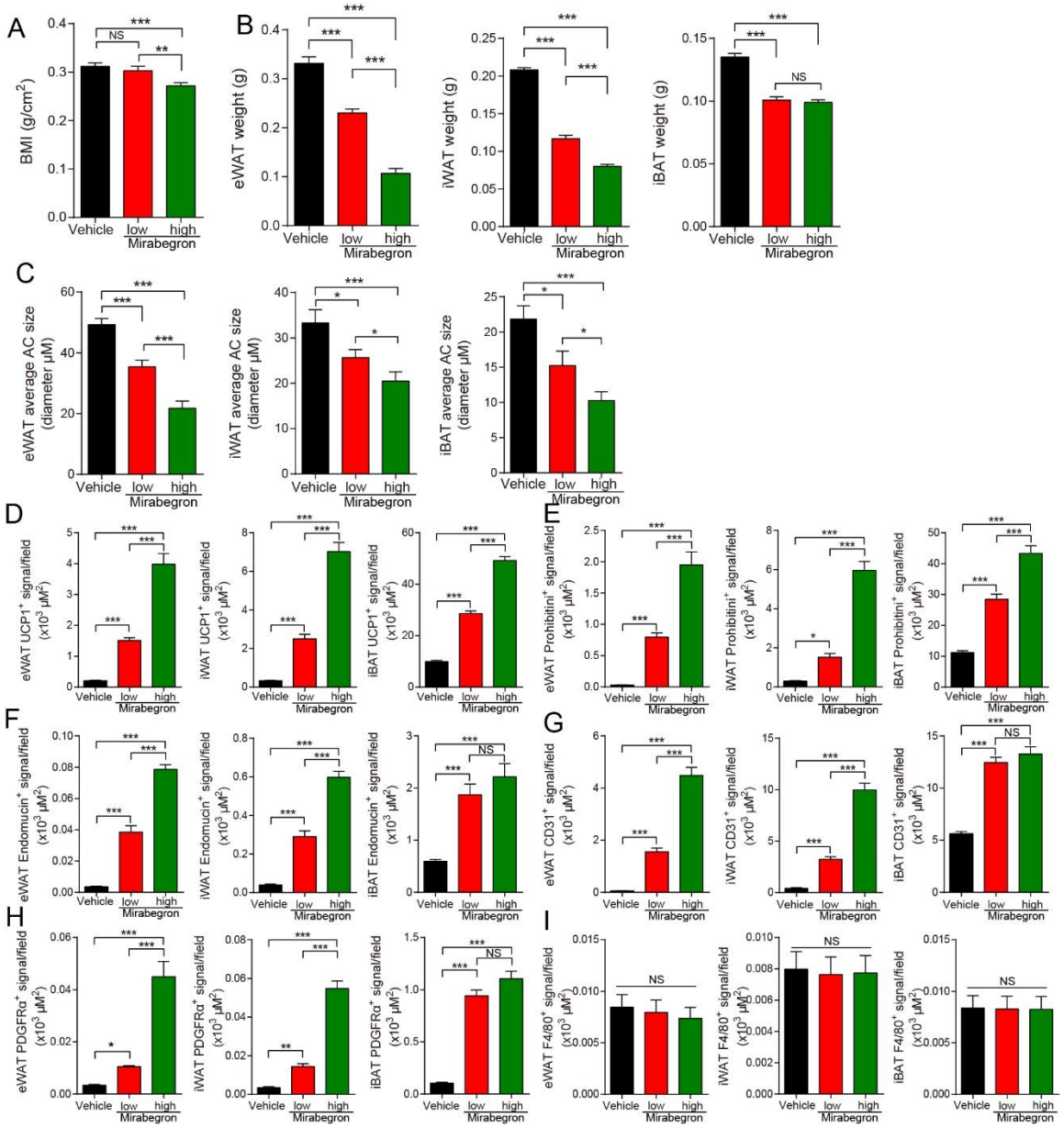

Fig. S1. The impact of mirabegron on BMI, adipose deposition and immunohistological analysis of mirabegron-treated adipose tissues.

A. The impact of 6-week treatment on BMI with mirabegon at low and high doses (n = 15 animals per group). NS = not significant; **p<0.01; ***p<0.001.

B. Adipose weight of iBAT, iWAT and eWAT after 6-week treatment with mirabegron (n = 15 per group). NS = not significant; ***p<0.001.

C. Quantification of average adipocyte size (n = 15 random fields from 5 mice per group). NS = not significant; *p<0.05; ***p<0.001.

D-I. Quantification of UCP1, prohibitin, endomucin, CD31, PDGFRα and F4/80 positive signals in Fig. 2 (n = 15 random fields from 5 mice per group). NS = not significant; *p<0.05; **p<0.01; ***p<0.001.

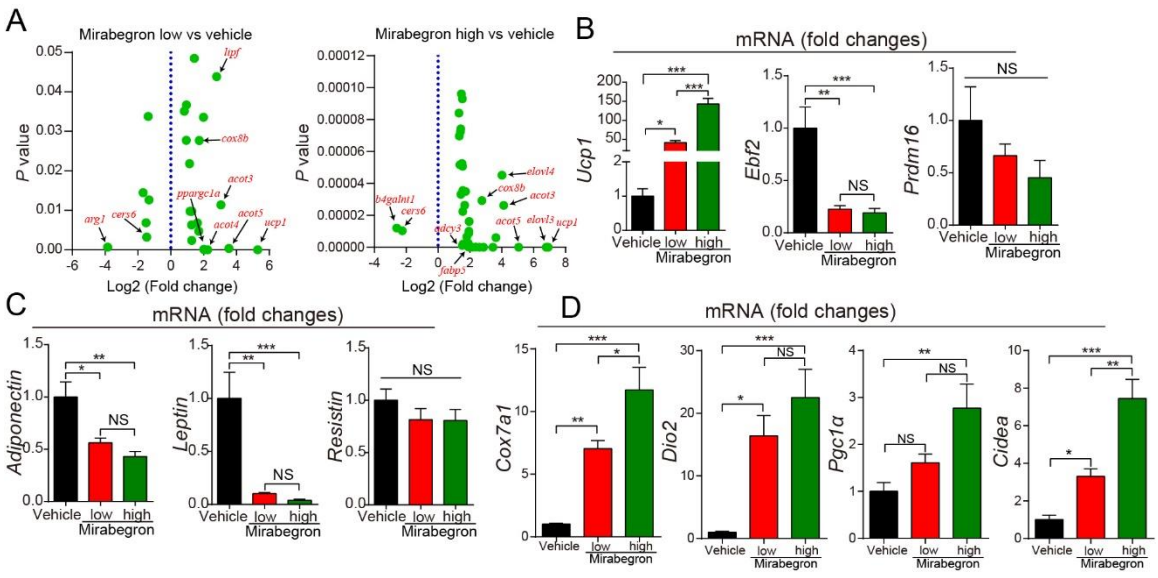

Fig. S2. Genome-wide expression profiling of mirabegron-treated iWAT and browning markers.

A. Volcano plots of lipolysis-related genes in mirabegron-treated WAT (n = 3 samples per group).

B and C. qPCR validation of *Ucp1, Ebf2, Prdm16, Adiponectin, Leptin* and *Resistin* expression in mirabegron-treated WAT (n = 6 samples per group). NS = not significant; **p*<0.05; ***p*<0.01; ****p*<0.001.

D. qPCR validation of *Cox7a1, Dio2, Pgc1α* and *Cidea* expression in mirabegron-treated WAT (n = 6 samples per group). NS = not significant; **p*<0.05; ***p*<0.01; ****p*<0.001.

Fig. S3. Gene ontology and Kyoto encyclopedia classification of the 30 top up-regulated genes in mirabegron-treated WAT.

A and **B**. The top 30-upregulated genes were classified according to their functions related to metabolism, lipolysis, and signaling pathways. Gene names are indicated in each panel.

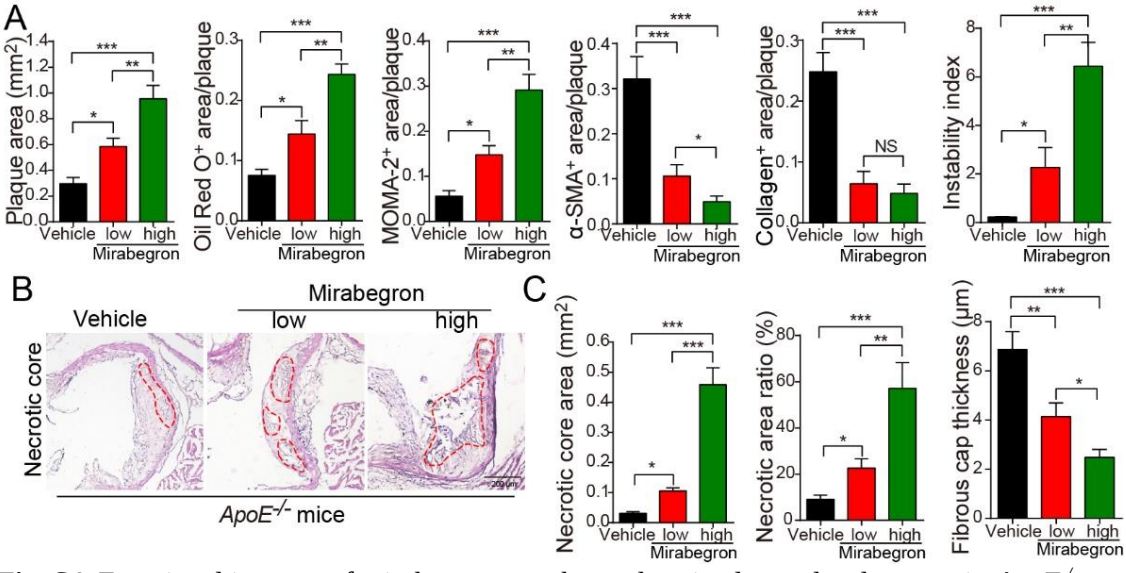

Fig. S4. Functional impacts of mirabegron on atherosclerotic plaque development in *ApoE*$^{-/-}$ mice.

A. Quantifications of plaque area and positive signals of oil red O, MOMA-2, α-SMA, Sirius red or plaque instability index of Fig. 4B (n = 6 samples per group). NS = not significant; **p*<0.05; ***p*<0.01; ****p*<0.001.
B. The necrotic core area of *ApoE*$^{-/-}$ mice plaques is encircled by dashed lines.
C. Quantification of average necrotic core areas in **B**. Quantification of the ratio of the necrotic core area versus the total plaque area and the fibrous cap thickness (n = 6 samples per group).

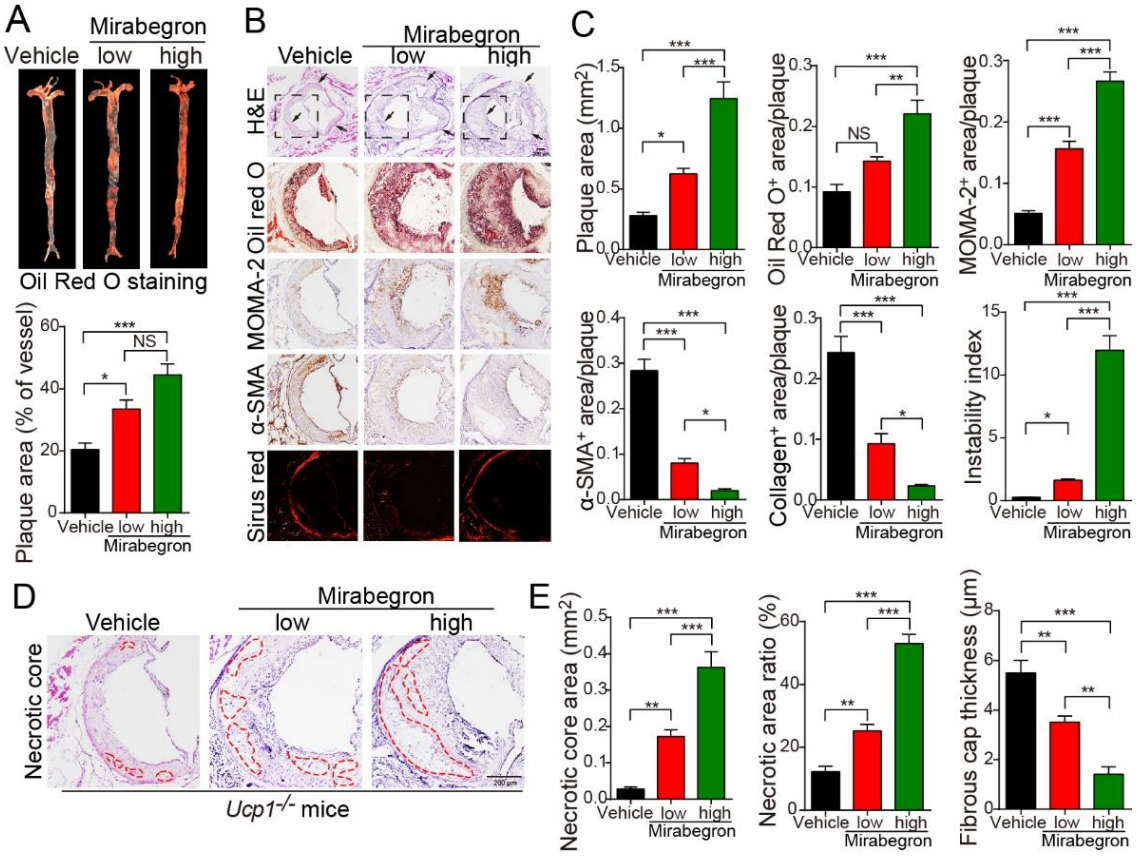

Fig. S5. Functional impacts of mirabegron on atherosclerotic plaque development in *Ldlr*$^{-/-}$ mice.
A. Gross examination and quantification of oil red O-stained aorta stem from mirabegron-treated and vehicle-treated *Ldlr*$^{-/-}$ mice (n = 6 samples per group).
B. Histological examination of cross-section of aorta roots from mirabegron-treated and vehicle-treated *Ldlr*$^{-/-}$ mice. Aorta sections were stained with H&E, oil red O, MOMA-2, α-SMA, or Sirius red. The boxed area the H&E-stained sections were amplified. Arrows point to the plaques.
C. Quantifications of plaque area and positive signals of oil red O, MOMA-2, α-SMA, Sirius red or plaque instability index (n = 6 samples per group). **p*<0.05; ***p*<0.01; ****p*<0.001.
D. The necrotic core area of *Ucp1*$^{-/-}$ mice plaques is encircled by dashed lines.
E. Quantification of average necrotic core areas in **D**. Quantification of the ratio of the necrotic core area versus the total plaque area and the fibrous cap thickness (n = 6 samples per group).

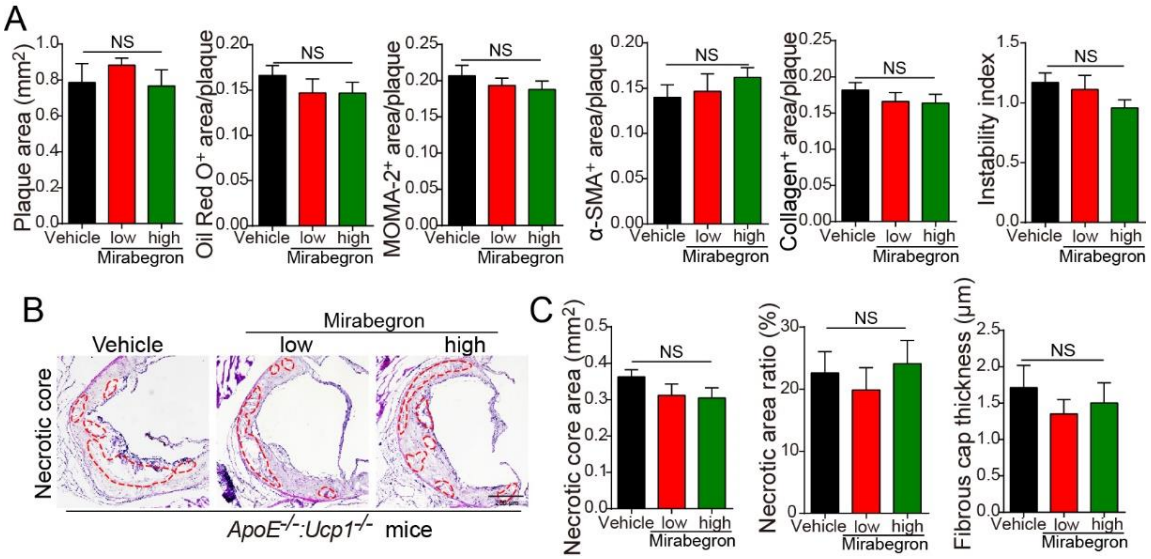

Fig. S6. Functional impacts of mirabegron on atherosclerotic plaque development in *ApoE*$^{-/-}$*:Ucp1*$^{-/-}$ mice.

A. Quantifications of plaque area and positive signals of oil red O, MOMA-2, α-SMA, Sirius red or plaque instability index of Fig. 6B (n = 6 samples per group).

B. The necrotic core area of *ApoE*$^{-/-}$*:Ucp1*$^{-/-}$ mice plaques is encircled by dashed lines.

C. Quantification of average necrotic core areas in **B**. Quantification of the ratio of the necrotic core area versus the total plaque area and the fibrous cap thickness (n = 6 samples per group).

NS = not significant; **p*<0.05; ***p*<0.01; ****p*<0.001.

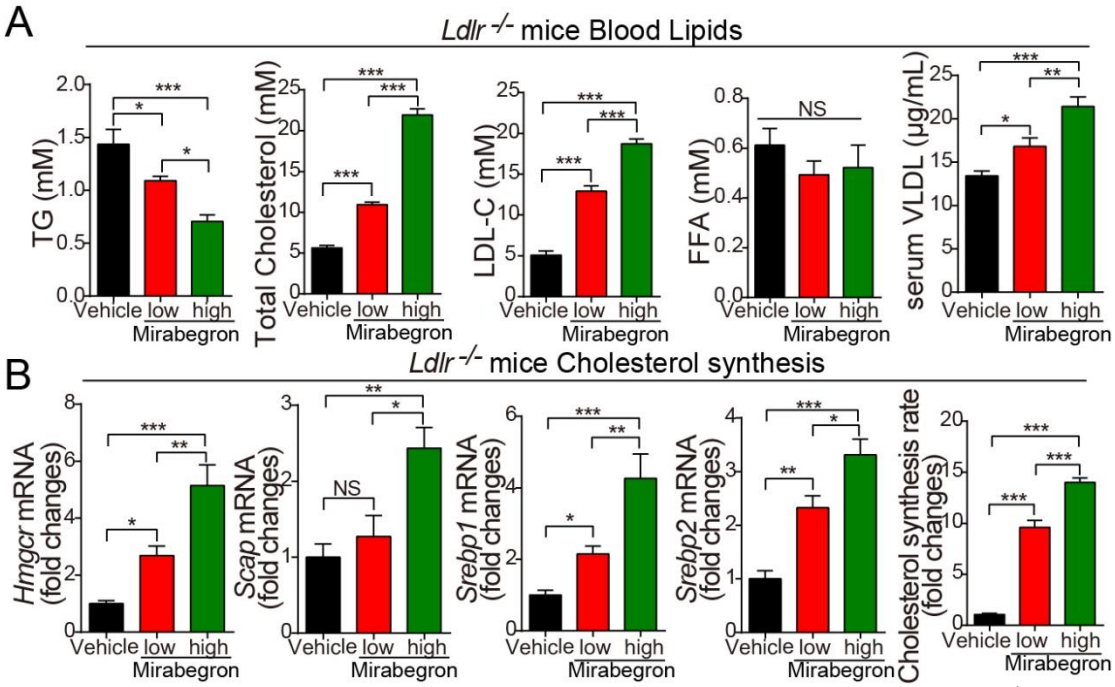

Fig. S7. Blood chemistry analysis and lipid profiling of mirabegron-treated *Ldlr*$^{-/-}$ mice.

A. Serum levels of TG, total cholesterol, LDL-C, FFA and VLDL in mirabegron- and vehicle-treated *Ldlr* $^{-/-}$ mice (n = 8 animals per group).

B. Analysis of cholesterol synthesis by qPCR quantification of liver *Hmgcr, Scap, Srebp1* and *Srebp2* expression levels in mirabegron- and vehicle-treated *Ldlr -/-* mice (n = 6 animals per group). NS = not significant; *p<0.05; **p<0.01; ***p<0.001.

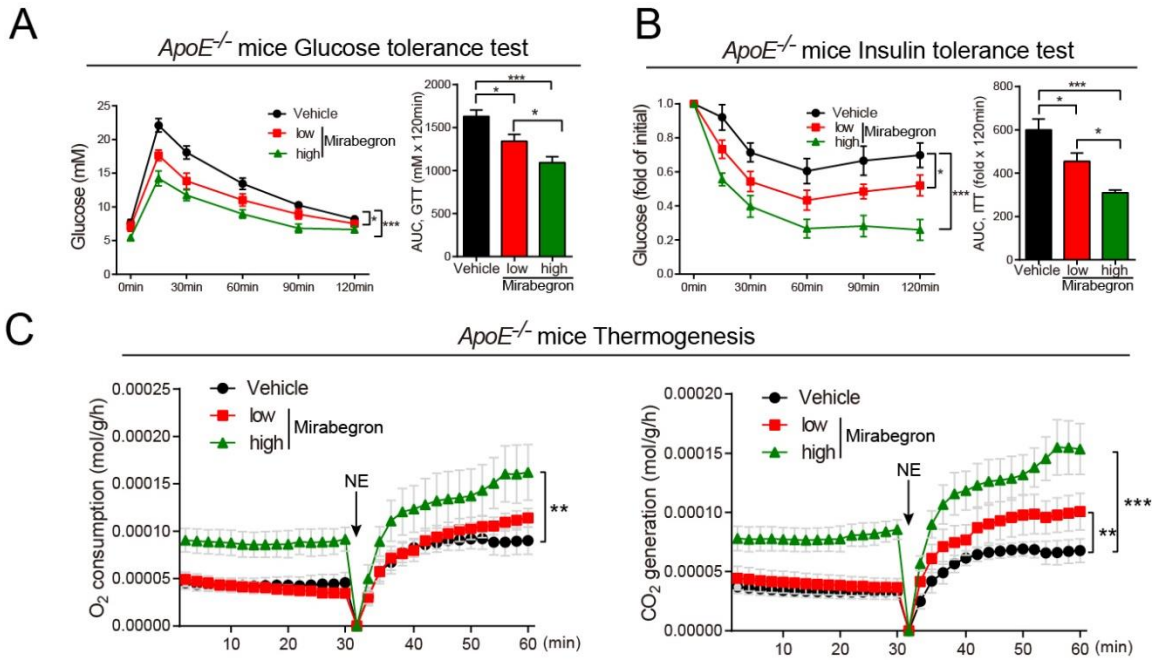

Fig. S8. Glucose and insulin tolerance test in mirabegron-treated *ApoE*$^{-/-}$ mice.

A. Glucose tolerance test in vehicle- and mirabegron-treated *ApoE*$^{-/-}$ mice (7 animals per group). The data of the AUC of glucose-tolerance test are also presented. *p<0.05; ***p<0.001.
B. Insulin tolerance test in vehicle- and mirabegron-treated *ApoE*$^{-/-}$ mice (6-10 animals per group). The data of the AUC of insulin-tolerance test are also presented. *p<0.05; ***p<0.001.
C. Metabolic measurements of the oxygen consumption rate and carbon dioxide production in response to norepinephrine in vehicle- and mirabegron-treated *ApoE*$^{-/-}$ mice (6 animals per group). **p<0.01; ***p<0.001.

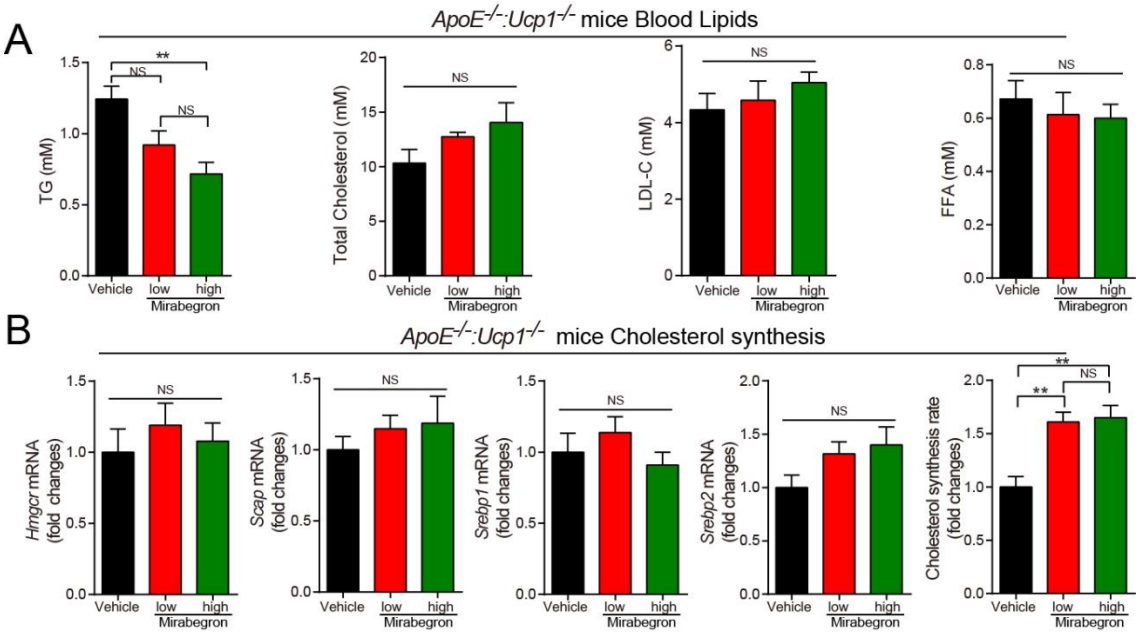

Fig. S9. Blood chemistry analysis and lipid profiling of mirabegron-treated *ApoE*$^{-/-}$*:Ucp1*$^{-/-}$ double knockout mice.

A. Serum levels of TG, total cholesterol, LDL-C, and FFA in mirabegron- and vehicle-treated *ApoE*$^{-/-}$*:Ucp1*$^{-/-}$ double knockout mice (n = 6 animals per group).
B. Analysis of cholesterol synthesis by qPCR quantification of liver Hmgcr, Scap, Srebp1 and Srebp2 expression levels in mirabegron- and vehicle-treated *ApoE*$^{-/-}$*:Ucp1*$^{-/-}$ double knockout mice (n = 6 animals per group). NS = not significant; ** $p<0.01$;

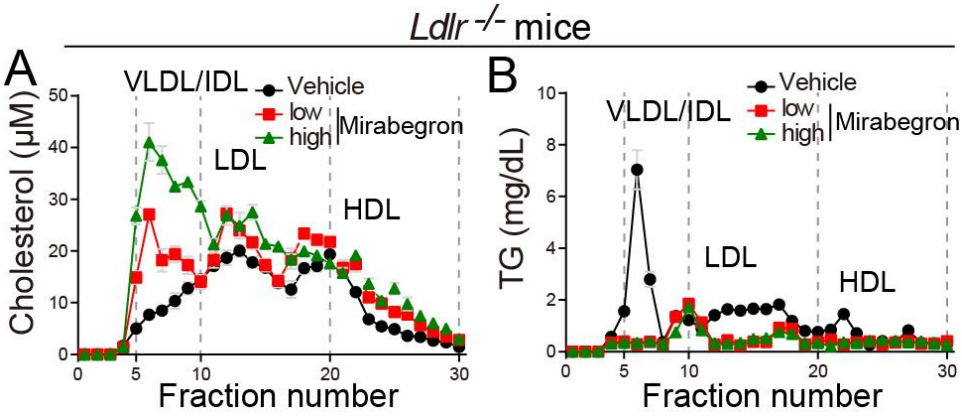

Fig. S10. FPLC analysis of plasma cholesterols.
A-B. Plasma cholesterol and TG levels of the mirabegron- and vehicle-treated *Ldlr*$^{-/-}$ mice (n = 6 animals per group). Values from fractions 5-10 were used for calculation of VLDL/IDL, whereas fractions 11-19 and fractions 20-30 represent LDL and HDL respectively.

Table S1. Primers for Real Time PCR.

Primer	Sequence 5'-3'
Adiponectin-forward	GTTCCCAATGTACCCATTCGC
Adiponectin-reverse	TGTTGCAGTAGAACTTGCCAG
Cidea-forward	TGACATTCATGGGATTGCAGAC
Cidea-reverse	GGCCAGTTGTGATGACTAAGAC
Dio2-forward	AATTATGCCTCGGAGAAGACCG
Dio2-reverse	GGCAGTTGCCTAGTGAAAGGT
Ebf2-forward	GGGATTCAAGATACGCTAGGAAG
Ebf2-reverse	GGAGGTTGCTTTTCAAAATGGG
Gapdh-forward	AGGTCGGTGTGAACGGATTTG
Gapdh-reverse	TGTAGACCATGTAGTTGAGGTCA
Hmgcr-forward	TGTTCACCGGCAACAACAAGA
Hmgcr-reverse	CCGCGTTATCGTCAGGATGA
Leptin-forward	GAGACCCCTGTGTCGGTTC
Leptin-reverse	CTGCGTGTGTGAAATGTCATTG
*Pgc1*α-forward	TATGGAGTGACATAGAGTGTGCT
Pgc1α-reverse	CCACTTCAATCCACCCAGAAAG
Prdm16-forward	CCACCAGCGAGGACTTCAC
Prdm16-reverse	GGAGGACTCTCGTAGCTCGAA
Resistin-forward	AAGAACCTTTCATTTCCCCTCCT
Resistin-reverse	GTCCAGCAATTTAAGCCAATGTT
Scap-forward	CCGAGCATTCCAACTGGTG
Scap-reverse	CCATGTTCGGGAAGTAGGCT
Srebp1-forward	TGACCCGGCTATTCCGTGA
Srebp1-reverse	CTGGGCTGAGCAATACAGTTC
Srebp2-forward	GCAGCAACGGGACCATTCT
Srebp2-reverse	CCCCATGACTAAGTCCTTCAACT
Ucp1-forward	AGGCTTCCAGTACCATTAGGT
Ucp1-reverse	CTGAGTGAGGCAAAGCTGATTT

References

1. Seki T, *et al.* (2016) Endothelial PDGF-CC regulates angiogenesis-dependent thermogenesis in beige fat. *Nat Commun* 7:12152.
2. Xue Y, *et al.* (2009) Hypoxia-independent angiogenesis in adipose tissues during cold acclimation. *Cell Metab* 9(1):99-109.
3. Dong M, *et al.* (2013) Cold exposure promotes atherosclerotic plaque growth and instability via UCP1-dependent lipolysis. *Cell Metab.* 18(1):118-129.
4. Honek J, *et al.* (2014) Modulation of age-related insulin sensitivity by VEGF-dependent vascular plasticity in adipose tissues. *Proc Natl Acad Sci U S A* 111(41):14906-14911.